RSC Advances

ROYAL SOCIETY OF CHEMISTRY

www.rsc.org/advances

A thermodynamic inclusion complex between TMeQ[6] with 4- pyrrolidinopyridine has been formed, and the unthreading and rethreading of the TMeQ[6] ring can simulate a molecular-level plug/socket system with *N*-butyl-4-pyrrolidinopyridine, which can be reversibly driven by Ba^{2+}/SO_4^{2-}.

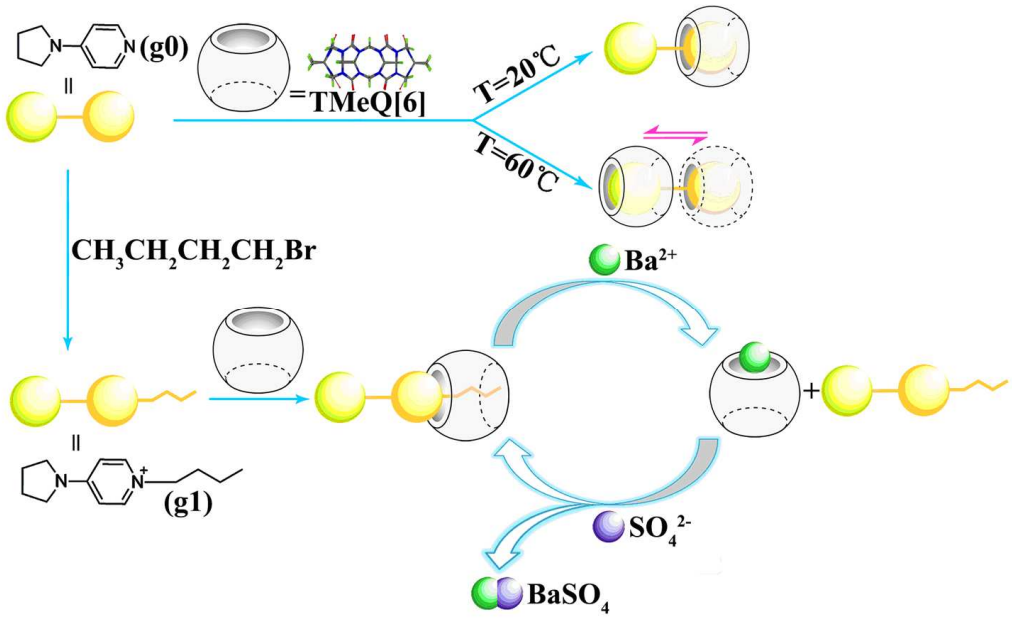

Cite this: DOI: 10.1039/c0xx00000x

www.rsc.org/xxxxxx

ARTICLE TYPE

Inclusion of 4-pyrrolidinopyridine derivatives in a symmetrical α,α',δ,δ'-tetramethyl-cucurbit[6]uril and a Ba^{2+}-driven pseudorotaxane with characteristic UV absorption changes

Bo Yang,[a] Xin Xiao,*[a] Yun-Qian Zhang,[a] Qian-Jiang Zhu,[a] Sai-Feng Xue,[a] Zhu Tao,[a] and Gang Wei*[b]

Received (in XXX, XXX) Xth XXXXXXXXX 20XX, Accepted Xth XXXXXXXXX 20XX
DOI: 10.1039/b000000x

The host–guest interactions between a symmetrical α,α',δ,δ'-tetramethyl-cucurbit[6]uril and three 4-pyrrolidinopyridine derivatives, specifically 4-pyrrolidinopyridine, *N*-butyl-4-pyrrolidinopyridine, and *N*-amyl-4-pyrrolidinopyridine, have been investigated both in aqueous solution and in the solid state using NMR spectroscopic methods, electronic absorption spectroscopy, isothermal titration calorimetry (ITC), and single-crystal X-ray diffraction analysis. In aqueous solution, TMeQ[6] forms 1:1 inclusion complexes with these guests. Generally, TMeQ[6] preferentially accommodates the pyridyl moiety of these guests, which was confirmed by the crystal structures of its complexes with 4-pyrrolidinopyridine and *N*-butyl-4-pyrrolidinopyridine. Moreover, TMeQ[6] can form a thermodynamic inclusion complex with 4-pyrrolidinopyridine at elevated temperatures. The unthreading and rethreading of the TMeQ[6] ring can simulate a molecular-level plug/socket system, that can be reversibly driven by Ba^{2+}/SO_4^{2-}, and is accompanied by obvious changes in the UV absorption spectrum, both in wavelength and intensity.

Introduction

Molecular motions are quite common in biosystems and closely related to macroscopic motions.[1-3] Inspired by the dynamic and reversible nature of natural supramolecular assemblies, scientists have applied artificial supramolecular architectures to mimic and control molecular motions.[4-8] Rotaxanes, considered as a typical type of mechanically interlocked structures, are crucial precursors for the fabrication of advanced supramolecular architectures[9-15] and have been widely used as building blocks to fabricate molecular shuttles and switches that show molecular motions induced by certain stimuli.[16-20] Though many well-known molecular recognition motifs,[21-23] such as crown ether/ammonium salt recognition couples, have been applied to investigate rotaxane-based molecular motions, the introduction of new molecular recognition motifs in the realm of rotaxanes will undoubtedly expand the applications of rotaxanes and show some unique stimuli responsiveness. [24-26] As new members of the functional macrocyclic family, supramolecular architectures.[27-33] However, due to the difficulty of their synthesis, substituted cucurbit[*n*]urils have only been applied to a limited extent in studies of molecular motions. In one of our previous works, we reported the synthesis and characterization of symmetrical α,α',δ,δ'-tetramethyl cucurbit[6]uril (TMeQ[6], Fig. 1),[34] which showed improved solubility compared to the unsubstituted Q[6] in water due to the increased molecular polarity associated with its lower molecular symmetry, leading to easier interaction with guests in aqueous media. In another previous work, we found that a cucurbit[6]uril can complex pyrrole salts, pyridine salts or alkyl chains with high binding constants.[35-41] For the present study, we have selected TMeQ[6] and three 4-pyrrolidinopyridine derivatives, namely 4-pyrrolidinopyridine (g0), *N*-butyl-4-pyrrolidinopyridine (g1), and *N*-amyl-4-pyrrolidinopyridine (g2), as basic building blocks. These have been used to synthesize a TMeQ[6]-based rotaxane, and we have examined the temperature/cation-controllable molecular motions of the TMeQ[6] ring on the 4-pyrrolidinopyridine axle.

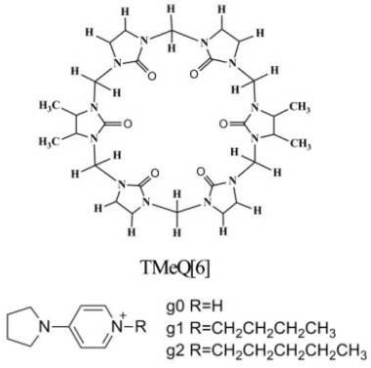

Fig. 1 Structures of TMeQ[6] and the 4-pyrrolidinopyridine derivatives (g0, g1, g2).

[a] *Key Laboratory of Macrocyclic and Supramolecular Chemistry of Guizhou Province, Guizhou University, Guiyang, 550025, People's Republic of China. E-mail: gyhxxiaoxin@163.com*
[b] *CSIRO Materials Science and Engineering, PO Box 218, Lindfield, NSW 2070, Australia. E-mail: gang.wei@csiro.au*

Results and discussion

4-pyrrolidinopyridine derivatives have multiple active sites, that is tetrahydropyrrole, pyridyl, and alkyl moieties, which may interact with a TMeQ[6] host. This could result in the formation of multiple supramolecular assemblies under different interaction conditions. In this study we have found that a thermodynamic arrangement of 4-pyrrolidinopyridine and TMeQ[6], whereas the other 4-pyrrolidinopyridine derivatives formed simple 1:1 inclusion host–guest complexes.

1:1 TMeQ[6]-based inclusion host–guest complexes

Simple 1:1 inclusion host–guest complexes were formed between TMeQ[6] and the guests with alkyl tails (g1 and g2). The interaction of the g1/TMeQ[6] complex could be conveniently monitored by ^{1}H NMR in D_2O. Fig. 2 shows the ^{1}H NMR spectra of g1 in D_2O recorded in the absence of TMeQ[6] (A), with 1.34 equivalents of TMeQ[6] (B) and neat TMeQ[6] in D_2O (C). An apparent upfield shift of the signals of the protons of alkyl chain and an obvious downfield shift of the signals of the protons closest to the pyridine N were observed as TMeQ[6] was added (Fig. 2B). The resonances of protons H_e, H_f, H_g, and H_h of the alkyl chain of g1, showed upfield shifts of 0.60, 0.80, 0.76 and 0.73 ppm, respectively, compared to those of unbound g1, and the resonance of protons H_d closest to the pyridine N of g1 showed a downfield shift of 0.67 ppm compared to that of the unbound g1. Similar ^{1}H NMR spectra for the interaction of TMeQ[6] and guest g2 were also recorded (Fig. S1 ESI†). This indicates that the alkyl moiety of g2 was accommodated within the cavity of TMeQ[6] and the pyridine ring was at its portal.

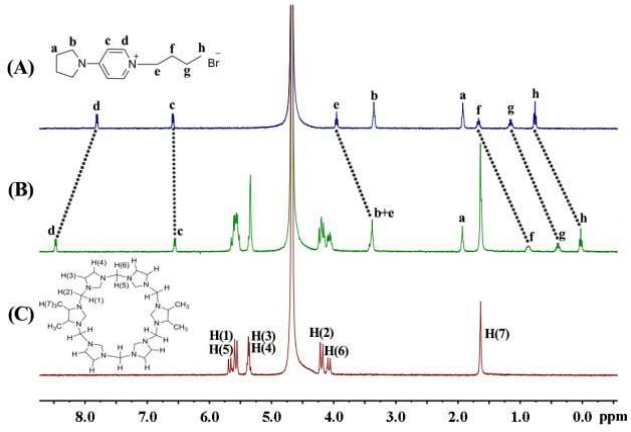

Fig. 2 Interaction of g1 and TMeQ[6]: ^{1}H NMR spectra (400 MHz, D_2O) of (A) g1 (ca. 2 mM) in the absence TMeQ[6], (B) in the presence of 1.34 equiv of TMeQ[6], and (C) neat TMeQ[6].

The interaction of TMeQ[6] with g1 was also examined by UV absorbance spectrophotometry (Fig. 3A). Upon addition of TMeQ[6], the complexation of g1 was followed by an increase in absorption with a bathochromic shift from 290 to 285 nm and an isosbestic point at 285 nm up to a 1:1 host–guest ratio (Fig. 3B and insert of Fig. 3C), which indicated the formation of a simple host–guest complex. The binding constant for the TMeQ[6]·g1 complex was $(4.38\pm0.03)\times10^5$ L mol^{-1}. Similar changes in the absorption spectra of the guest g2 were observed with increasing TMeQ[6] concentration, and the binding constant for the TMeQ[6]·g2 complex was $(1.77\pm0.03)\times10^6$ L mol^{-1} (Fig. S2 ESI†).

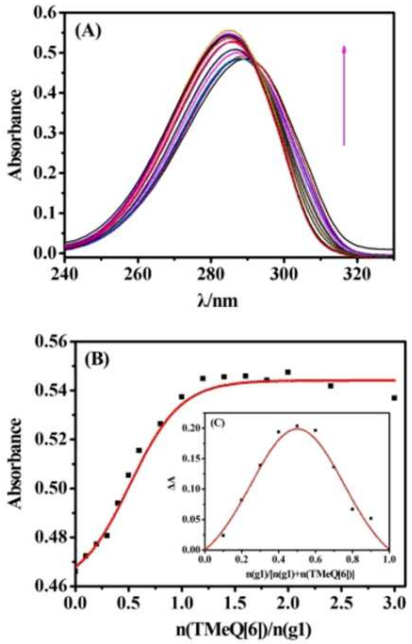

Fig. 3 Interaction of g1 and TMeQ[6]: (A) absorption spectra of g1 (20 μM) in aqueous solution at different TMeQ[6] concentrations, (B) concentrations and the corresponding A vs $N_{TMeQ[6]}/N_{g1}$ curve and (C) concentrations and the corresponding ΔA vs $N_{g1}/(N_{TMeQ[6]}+N_{g1})$ curve (inset).

Isothermal titration calorimetry (ITC) experiments were also performed to quantitatively determine the association constant (Ka) of TMeQ[6] with g1 as $(4.23\pm0.6)\times10^5$ M^{-1} (Fig. 4), fitted by using the "Independent" model, suggesting a strong binding of TMeQ[6] with the guest g1, and the experimental "n" value was 0.935±0.01, suggesting that the interaction ratio of the host and guest was 1:1, consistent with the results from UV absorbance spectrophotometry. Similar ITC experimental results between TMeQ[6] and guest g2 were also recorded (Fig. S3 and Table S1, ESI†), whereas the larger binding constant [$(1.08\pm0.32)\times10^6$ M^{-1}] suggested that the complex of TMeQ[6]·g2 was more stable than complex of TMeQ[6]·g1.

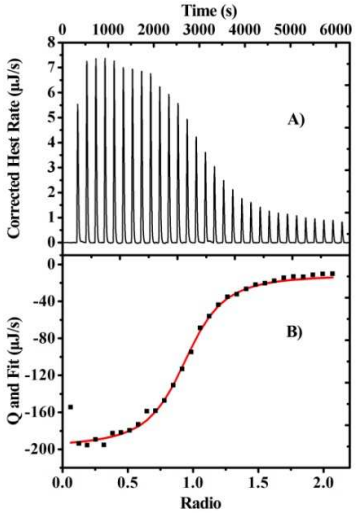

Fig. 4 Isothermal titration calorimetry profiles of TMeQ[6] with g1 in aqueous solution at 298.15 K. A) Nano ITC data for 30 sequential injections (each of 6 mL) of g1 solution (1.0 mM) into TMeQ[6] solution (0.1 mM). B) Apparent reaction heat obtained from integration of the calorimetric traces.

Slow evaporation of the volatiles from an aqueous solution containing the host TMeQ[6] and the guest g1 in a 1:1 ratio produced X-ray quality single crystals, which crystallized in the triclinic system with space group *P*-1. Single-crystal diffraction analysis showed the structure of the inclusion complex of TMeQ[6]·g1, in which the alkyl chain of the g1 guest is located inside the cavity of the TMeQ[6] host, whereas the other section of the g1 guest remains outside of the portal (Fig. 5). The ionic dipole interaction between the positive nitrogen (N26) of the pyridyl moiety of g1 and the portal carbonyl oxygens of TMeQ[6] and the hydrophobic interaction of the cavity of TMeQ[6] with the alkyl chain of g1 could be the driving forces for the formation of such an inclusion complex. The Average $N_{pyridyl}\cdots O_{carbonyl}$ short-distance is 3.728 Å.

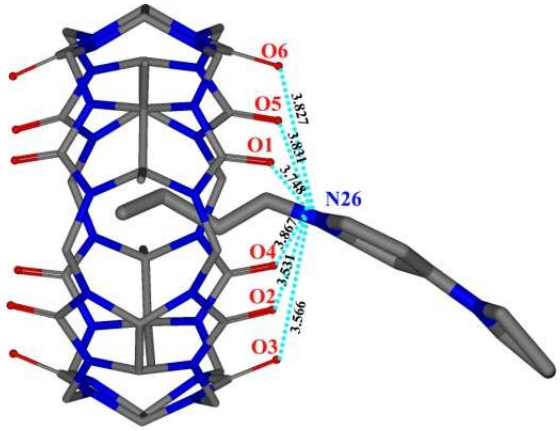

Fig. 5 ORTEP diagram of the inclusion complex TMeQ[6]·g1 in side view.

Generally, the portal carbonyl oxygens of cucurbit[*n*]urils coordinate with metal cations through mainly the ion-dipole interactions. In aqueous solution, the association constant (*K*a) of Q[6] with Ba^{2+} is 1.7×10^5 M^{-1}. ITC measurement showed an association constant of *K*a = $(4.91\pm0.8)\times10^5$ M^{-1} for TMeQ[6] with Ba^{2+} (Table 1 and Fig. 6), similar to that of TMeQ[6] with g1. Therefore, there may be a competitive interaction between g1 and Ba^{2+} with TMeQ[6]. When 100 equivalents of barium chloride was added to a solution of TMeQ[6]·g1 pseudorotaxane (2×10^{-5} M of g1 with 1.0 equivalent of TMeQ[6]), the absorption spectrum of the solution was essentially the same as that of neat g1 (2×10^{-5} M, Fig. 7A). However, Li_2SO_4 (300 equivalents) had a slight influence on the absorption spectrum of the same pseudorotaxane system (2×10^{-5} M of g1 with 1.0 equivalent of TMeQ[6]). When barium chloride (300 equivalents) was added to this solution, the absorption spectrum essentially returned to that of the 2×10^{-5} M solution of g1 once more. Dissociation and regeneration of the pseudorotaxane have been verified by repeating the process of adding $BaCl_2$ and Li_2SO_4 (Fig. 7B).

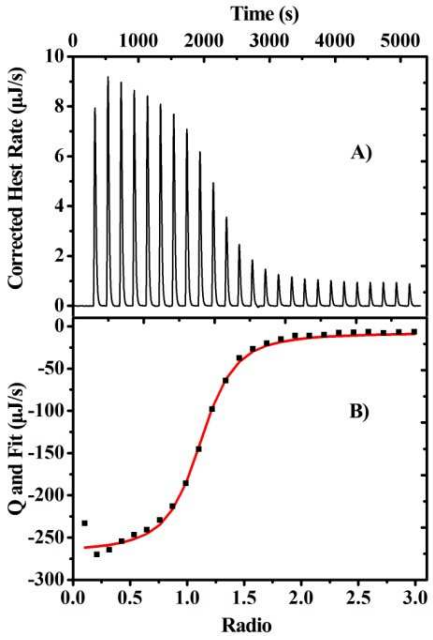

Fig. 6 Isothermal titration calorimetry profiles of TMeQ[6] with $BaCl_2$ in aqueous solution at 298.15 K. A) Nano ITC data for 30 sequential injections (each of 6 mL) of $BaCl_2$ solution (1.0 mM) into TMeQ[6] solution (0.1 mM). B) Apparent reaction heat obtained from integration of the calorimetric traces.

Table 1 Microcalorimetric titration data for TMeQ[6] with $BaCl_2$ in aqueous solution at 298.15 K.

Complex	*n*	*Ka* (M^{-1})	*ΔH*(kJ mol^{-1})	*TΔS*(kJ mol^{-1})
$BaCl_2$+TMeQ[6]	1.08±0.01	$(4.91\pm0.80)\times10^5$	–25.99±0.50	6.49

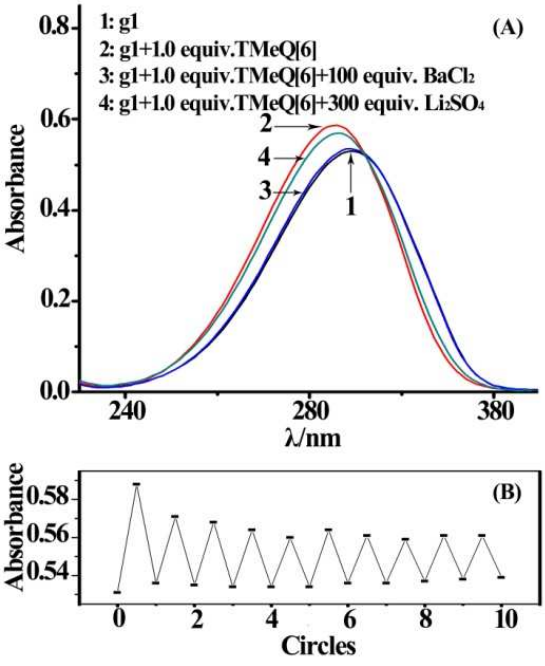

Fig 7 Absorption spectra of aqueous solutions of compound g0 (2×10^{-5} M) under different conditions(A) and plot of experimental data on the reversibility of Ion-driven dissociation – regeneration of pseudorotaxane (B): Absorption intensity at the maximum absorption wavelength.

A thermodynamic arrangement

A thermodynamic arrangement was found between TMeQ[6] and guest g0. Formation of the g0·TMeQ[6] complex could be conveniently monitored by ^{1}H NMR in D_2O at 20 and 60°C. Fig. 8 shows the ^{1}H NMR titration spectra of g0 in D_2O recorded in the absence of TMeQ[6](A) and with increasing proportions of TMeQ[6] at 0.47 (B), 0.86 (C), 1.29 (D), and 1.31 equiv. (E) at 20°C. Only one set of undeuterated protons of g0 showed a gradual upfield or downfield shift with increasing number of equivalents of TMeQ[6] (from bottom to top), suggesting that TMeQ[6] can incorporate g0 into its cavity with a fast ingress and egress exchange rate. Upon the addition of TMeQ[6], the signals of protons H_c and H_d of the pyridine ring of g0 showed upfield shifts while that of protons H_a of the pyrrole ring of g0 showed essentially no change. The signal of protons H_b closest to the pyrrole N of g0 showed a downfield shift. At 1.29 equiv of TMeQ[6], the resonances of protons H_d, H_c, and H_a of g0, showed upfield shifts of 0.94, 0.23, and 0.07 ppm, while that of the protons H_b of g0 showed downfield shift of 0.24 ppm compared to the positions in free g0. However, obvious differences for the host–guest inclusion complex of TMeQ[6]·g0 were seen in ^{1}H NMR experiments in D_2O at 60°C. Fig. 9 shows ^{1}H NMR titration spectra of g0 in D_2O recorded with the absence of TMeQ[6] (A) and in increasing proportions of TMeQ[6] at 0.72 (B), 0.77 (C), 0.83 (D), and 0.97 (E). Upon the addition of TMeQ[6], the signals of all the protons H_a, H_b, H_c, and H_d of g0 showed upfield shifts. At 0.97 equiv of TMeQ[6], the resonances of protons H_d, H_c, H_b ,and H_a of g0, showed upfield shifts of 0.82, 0.37, 0.14 and 0.30 ppm, respectively, compared to those in the free g0. This indicates that the pyridine ring was accommodated in the cavity of TMeQ[6] at 20°C. However, at 60°C, TMeQ[6] could shuttle on the guest g0 in a state of dynamic equilibrium.

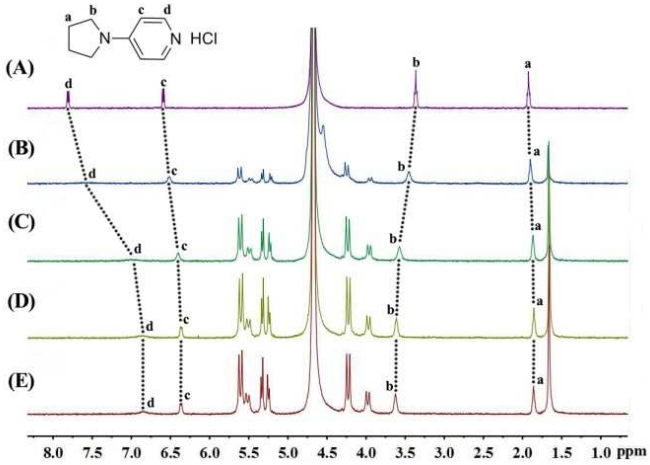

Fig. 8 Interaction of g0 and TMeQ[6] (20°C): ^{1}H NMR spectra (400 MHz, D_2O) of g0 (ca. 2 mM) in the absence of TMeQ[6] (A), in the presence of 0.47 equiv of TMeQ[6] (B), in the present of 0.86 equiv of TMeQ[6] (C), in the present of 1.29 equiv of TMeQ[6] (D), and in the present of 1.31 equiv of TMeQ[6] (E).

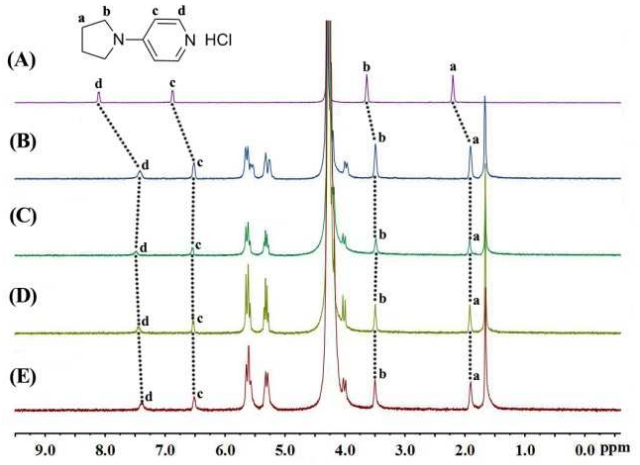

Fig. 9 Interaction of g0 and TMeQ[6] (60 °C): ^{1}H NMR spectra (400 MHz, D_2O) of g0 (ca. 2 mM) in the absence of TMeQ[6] (A), in the presence of 0.72 equiv of TMeQ[6] (B), in the present of 0.77 equiv of TMeQ[6] (C), in the present of 0.83 equiv of TMeQ[6] (D), and in the present of 1.05 equiv of TMeQ[6] (E).

The TMeQ[6]:g0 interaction was also examined by UV absorbance spectrophotometry. With increasing amount of TMeQ[6], the absorbance of g0 was incrementally decreased at 282 nm (Fig. 10), indicating that g0 interacts with TMeQ[6]. The binding constant (*K*a) for the TMeQ[6]-g0 complex was $(6.90\pm0.09)\times10^3$ L mol^{-1}. Additionally, isothermal titration calorimetry (ITC) experiments were performed to quantitatively determine the association constant (*K*a) of TMeQ[6] with g0 as $(8.35\pm0.9)\times10^3$ M^{-1} (Fig. 11), fitted by using the "Independent" model, a relatively weak binding of TMeQ[6] to g0.

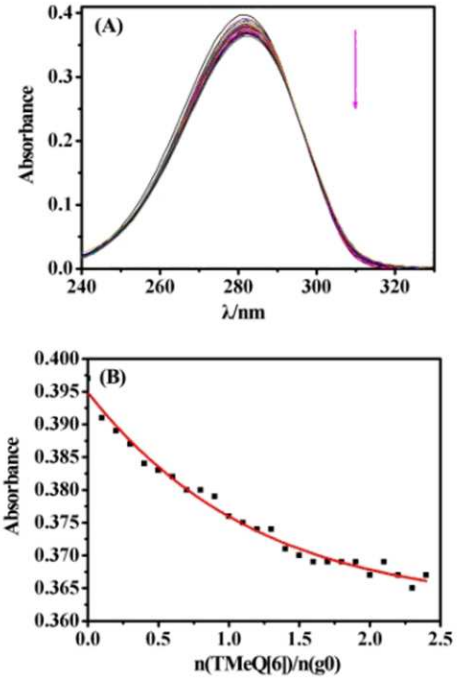

Fig. 10 Interaction of g0 and TMeQ[6]: absorption spectra of g0 (20 μM) in aqueous solution at different TMeQ[6] concentrations (A), and the corresponding A *vs* $N_{TMeQ[6]}/N_{g0}$ curve (B).

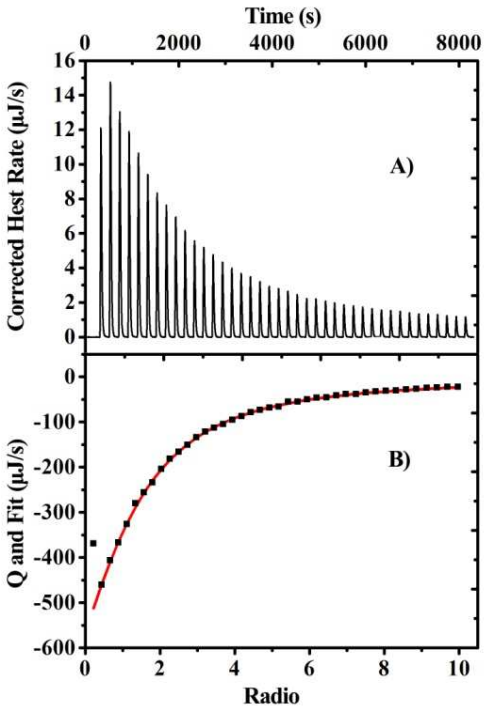

Fig. 11 Microcalorimetric titration of TMeQ[6] with g0 in aqueous solution at 298.15 K. A) Nano ITC data for 30 sequential injections (each of 6 mL) of $BaCl_2$ solution (7.0 mM) into TMeQ[6] solution (0.2 mM). B) Apparent reaction heat obtained from integration of the calorimetric traces.

Slow evaporation of the volatiles from an aqueous solution of host and the guest in a 1:1 ratio produced X-ray quality single crystals of the inclusion complex TMeQ[6]·g0, which crystallized in the triclinic system with space group *P*-1. The single-crystal structure of the inclusion complex TMeQ[6]·g0 showed a binding mode consistent with that in the solution state (Fig. 12), that is, the pyridine ring of the g0 guest is located in the cavity of the TMeQ[6] host, whereas the other part of the g0 guest remains outside of the portal. According to the p*K*a shift experimental results, protonated g0 exists over a wide pH range (at least between 2 and 8, and all experiments were performed at pH 5.) (see Fig. S4 ESI†). Thus, the proton on nitrogen N25 or N26 could interact with the portal carbonyl oxygens through hydrogen bonding, and additionally, the hydrophobic interaction of the TMeQ[6] cavity enhances the affinity for the pyridyl moiety of the guest g0. A combination of these interactions results in the formation of the TMeQ[6]·g0 inclusion complex. The average N(–H)…O hydrogen-bonding distance is 4.041 Å.

Thus, at the lower temperature, the TMeQ[6]·g0 inclusion complex formed shows a binding mode in which the pyridine moiety of g0 is accommodated in the cavity of TMeQ[6], whereas the tetrahydropyrrolidinyl moiety of g0 is held at the portal of TMeQ[6] (Fig. 13A). At the higher temperature, however, the TMeQ[6]·g0 inclusion complex formed shows a binding mode in which a TMeQ[6] molecule could shuttle on a guest g0 in a state of dynamic equilibrium (Fig. 13B).

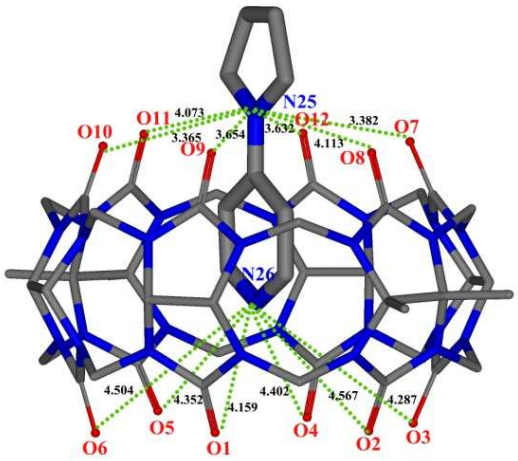

Fig. 12 ORTEP diagram of the inclusion complex TMeQ[6]·g0 in side view.

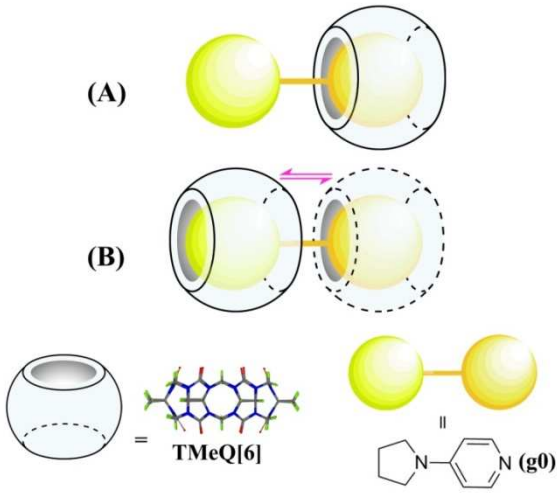

Fig. 13 The possible arrangement modes of TMeQ[6] with g0 in aqueous solution at different temperatures. (A) at 20°C, (B) at 60°C.

Conclusions

We have investigated the host–guest interactions of three guests (g0, g1, g2) with the macrocyclic host TMeQ[6] both in aqueous solution and in the solid state using NMR spectroscopic methods, electronic absorption spectroscopy, single-crystal X-ray diffraction analysis, and Isothermal Titration Calorimetry (ITC). The host–guest inclusion behavior of g1 in TMeQ[6] in aqueous solution is consistent with that in the solid state. The unthreading and rethreading of the TMeQ[6] ring can simulate a molecular-level plug/socket system The host–guest inclusion behavior of g2 in TMeQ[6] is similar to that of g1 in aqueous solution. However, the host–guest inclusion behavior of g0 in TMeQ[6] in aqueous solution is affected by temperature. At room temperature in aqueous solution, the host–guest inclusion behavior of g0 in TMeQ[6] shows multiple arrangement modes, whereas at 60°C it is consistent with that in the solid state. This observation not only contributes to a deeper understanding of the interactions between redox guests and macrocycle hosts, but may also expedite the design and construction of novel molecular machines. We are actively pursuing such opportunities strategies.

Experimental Section

Materials

4-pyrrolidinopyridine was purchased from Aldrich, and TMeQ[6] was prepared and purified according to previously published methods.[34] All other reagents were of analytical grade and were used as received. Double-distilled water was used for all experiments.

Synthesis of guest g1

4-pyrrolidinopyridine (0.25 g, 0.0017 mol) was dissolved in 1-Bromobutane (3 ml). The solution was stirred with a small magnetic stir bar under an inert nitrogen atmosphere and heated to 105 °C with an oil bath and refluxed for 12 h. The resulting solution was filtered and then the yellow precipitate was purified with Diethyl ether and dried in vacuum to give g1 (0.40 g, 82%). ^{1}H NMR (D_2O, 400 MHz) δ: 7.80 (d, J = 8 Hz, 2H), 6.58 (d, J = 8 Hz, 2H), 3.94 (t, J = 14 Hz, 2H), 3.33 (t, J = 12 Hz, 4H), 1.90 (t, J = 12 Hz, 4H), 1.65 (p, J = 30 Hz, 2H), 1.13 (q, J = 22 Hz, 2H), 0.73 (t, J=14 Hz, 3H). Anal. Calcd. for $C_{13}H_{21}N_2Br$: C, 54.74; H, 7.42; N, 9.82; found C, 54.69; H, 7.49; N, 9.96.

Synthesis of guest g2

Use of the same synthesis method as for g1 gave g2 (0.43 g, 85%). ^{1}H NMR (D_2O, 400 MHz) δ: 7.81 (d, J = 4 Hz, 2H), 6.59 (d, J = 8 Hz, 2H), 3.93 (t, J = 14 Hz, 2H), 3.35 (t, J = 13 Hz, 4H), 1.92 (t, J = 13 Hz, 4H), 1.69 (t, J = 29 Hz, 2H), 1.13 (d, J = 47 Hz, 4H), 1.23 (t, J = 14 Hz, 3H). Anal. Calcd. for $C_{14}H_{23}N_2Br$: C, 56.19; H, 7.75; N, 9.36; found C, 56.27; H, 7.69; N, 9.28.

Synthesis of the inclusion complex TMeQ[6]·g0

TMeQ[6] (6.2 mg, 0.005 mmol), g0 (1.8 mg, 0.010 mmol) and $CdCl_2·4H_2O$ (11.8 mg, 0.051 mmol) were dissolved in H_2O (3 mL). The mixture was heated until complete dissolution. Slow evaporation of the volatiles from the solution over a period of about two weeks provided colorless crystals.

Synthesis of the inclusion complex TMeQ[6] ·g1

TMeQ[6] (6.2 mg, 0.005 mmol), g1 (14.4 mg, 0.050 mmol) and $CdCl_2·2H_2O$ (11.8 mg 0.051 mmol) were dissolved in H_2O (3 mL). The mixture was heated until complete dissolution. Slow evaporation of the volatiles from the solution over a period of about two weeks provided colorless crystals.

^{1}H NMR measurements

To analyze the host–guest complexation of TMeQ[6] and g0/g1/g2, 2.0–2.5×10^{-3} mmol solutions of TMeQ[6] in 0.5–0.7 mL D_2O with TMeQ[6]: g0/g1/g2 ratios ranging between 0 and 2 were prepared, and the corresponding ^{1}H NMR spectra were recorded at 20 °C on a VARIAN INOVA-400 spectrometer. To analyze the host-guest complexation of TMeQ[6] and g0 at different temperature, the corresponding ^{1}H NMR spectra were recorded at 20 and 60 °C on a VARIAN INOVA-400 spectrometer.

UV-visible spectroscopy measurements

All UV-visible spectra were recorded from samples in 1 cm quartz cells on an Agilent 8453 spectrophotometer, equipped with a thermostat bath (Hewlett Packard, California, USA). The host and guests were dissolved in distilled water. UV-visible spectra were obtained at 25 °C at a concentration of 2.00×10^{-5} mol·L^{-1} gi (i=0,1,2) and different TMeQ[6] concentrations for the TMeQ[6]@gi (i=0,1,2) system.

ITC measurements

Microcalorimetric experiments were performed using an isothermal titration calorimeter Nano ITC (TA, USA). The experiments of g1 with TMeQ[6] and g2 with TMeQ[6] consisted of 30 consecutive injections (6 μL) of a guest solution into the microcalorimetric reaction cell (1 mL) charged with a solution of TMeQ[6]. The experiments of g0 with TMeQ[6] consisted of 40 consecutive injections (6 μL) of a guest solution into the microcalorimetric reaction cell (1 mL) charged with a solution of TMeQ[6] at 25 °C. The heat of reaction was corrected for the heat of dilution of the guest solution determined in separate experiments. All solutions were degassed prior to titration experiment by sonication . Computer simulations (curve fitting) were performed using the Nano ITC analyze software。

Crystal structure determination

Diffraction data for the inclusion complexes TMeQ[6]·g0 and TMeQ[6]·g1 were collected at 293 K with a Bruker SMART Apex-II CCD diffractometer using graphite-monochromated Mo-Kα radiation (λ=0.71073 Å). Absorption corrections were applied by using the multiscan program SADABS. Structural solution and full-matrix least-squares refinement based on F2 were performed with the SHELXS-97 and SHELXL-97 program packages, respectively. All non-hydrogen atoms were refined with anisotropic displacement parameters. The carbon-bound hydrogen atoms were introduced at calculated positions. All hydrogen atoms were treated as riding atoms with an isotropic displacement parameter equal to 1.2 times that of the parent atom. For the inclusion complexes TMeQ[6]·g0 and TMeQ[6]·g1, in these structures, the unit cell includes a large of isolated water molecules. We employed PLATON/SQUEEZE to calculate the diffraction contribution of the solvent molecules and, thereby, to produce a set of solvent-free diffraction intensities.

.

Crystal data for the inclusion complex TMeQ[6]·g0

$C_{138}H_{158}N_{76}O_{36}$, $F.W.$=3457.41, triclinic, space group P-1, a=14.6042(7) Å, b=18.9617(10) Å, c=22.6534(9) Å, α=96.608(4)°, β=104.969(4)°, γ=111.880(5)°, V=5465.3(4)Å^3, z=1, D_c=1.051 g cm^{-3}, F(000)=1806, GoF=1.009, R_{int}=0.0830, R_1 [I>2σ(I)] =0.1055, wR_2[I>2σ(I)]=0.2550, R_1(all data)=0.1932, wR_2(all data)=0.2819. CCDC 1012176.

Crystal data for the inclusion complex TMeQ[6]·g1

$C_{106}H_{130}N_{52}O_{30}Cd_3Cl_8$, $F.W.$=3233.45, triclinic, space group P-1, a=12.8214(6) Å, b=13.6444(13) Å, c=22.360(2) Å, α=82.000(8)°, β=86.425(5)°, γ= 87.378(6)°, V=3863.3(5) Å^3, z=1, D_c=1.390 g cm^{-3}, F(000)=1650, GoF=1.071, R_{int}=0.0483, R_1[I>2σ(I)] =0.1200, wR_2[I>2σ (I)]=0.2914, R_1(all data)=0.1539, wR_2(all data)=0.3270. CCDC 1012177.

Acknowledgements

Financial support from the National Natural Science Foundation

of China (NSFC; No. 21101037), and the International cooperation projects of Science and Technology Agency of Guizhou Province (Grant No. 20127005).

Notes and references

1 P. A. Kroon, M. Kainosho and S. I. Chan, *Nature*. 1975, **256**, 582–584.
2 H. Noji, R. Yasuda, M. Yoshida and K. Kinoshita, *Nature*. 1997, **386**, 299–302.
3 J. Howard, *Nature*. 1997, **389**, 561–567.
4 A. S. Lane, D. A. Leigh and A. Murphy, *J. Am. Chem. Soc*. 1997, **119**, 11092–11093.
5 G. Bottari, F. Dehez, D. A. Leigh, P. J. Nash, E. M. P´erez, J. K. Y. Wong and F. Zerbetto, *Angew. Chem. Int. Ed*. 2003, **42**, 5886–5889.
6 B. Lewandowski, G. D. Bo, J. W. Ward, M. Papmeyer, S. Kuschel, M. J. Aldegunde, P. M. E. Gramlich, D. Heckmann, S. M. Goldup, D. M. D'Souza, A. E. Fernandes and D. A. Leigh, *Science*. 2013, **339**, 189–193.
7 K. Zhu, V. N. Vukotic, N. Noujeim and S. J. Loeb, *Chem. Sci*. 2012, **3**, 3265–327.
8 C. G. Collins, E. M. Peck, P. J. Kramer and B. D. Smith, *Chem. Sci*. 2013, **4**, 2557–2563.
9 Y. Liu, H. Wang, P. Liang and H. Y. Zhang, *Angew. Chem. Int. Ed*. 2004, **43**, 2690–2694.
10 D. H. Qu, Q. C. Wang and H. Tian, *Angew. Chem. Int. Ed*. 2005, **44**, 5296–5299.
11 A. Harada, A. Hashidzume, H. Yamaguchi and Y. Takashima, *Chem. Rev*. 2009, **109**, 5974–6023.
12 S. Li, B. Zheng, J. Chen, S. Dong, Z. Ma, F. Huang and H. W. Gibson, *J. Polym. Sci. Part A: Polym. Chem.* 2010, **48**, 4067–4073;
13 W. Zhu, W. Li, C. Wang, J. Cui, H. Yang, Y. Jiang and G. Li, *Chem. Sci*. 2013, **4**, 3583–3590.
14 S. Dong, J. Yuan and F. Huang, *Chem. Sci*. 2014, **4**, 247–252.
15 Y. Yang, Y. Sun and N. Song, *Acc. Chem. Res.* 2014, doi.org/10.1021/ar500022f.
16 Z. Niu and H. W. Gibson, *Chem. Rev*. 2009, **109**, 6024–6046.
17 L. Fang, M. A. Olson, D. Ben´ıtez, E. Tkatchouk, W. A. Godddard and J. F. Stoddart, *Chem. Soc. Rev*. 2010, **39**,17–29.
18 L. Fang, M. A. Olson, D. Benítez, E. Tkatchouk, W. A. Godddard and J. F. Stoddart, *Chem. Soc. Rev*. 2010, **39**, 17–29.
19 V. N. Vukotic and S. J. Loeb, *Chem. Soc. Rev*. 2012, **41**, 5896–5906.
20 C. B. Caputo, K. Zhu, V. N. Vukotic, S. J. Loeb and D. W. Stephan, *Angew. Chem. Int. Ed*. 2013, **52**, 960–963.
21 W. C. Yount, H. Juwarker and S. L. Craig, *J. Am. Chem. Soc*. 2003, **125**, 15302–15303.
22 W. Weng, J. B. Beck, A. M. Jamieson and S. J. Rowan, *J. Am. Chem. Soc*. 2006, **128**, 11663–11672.
23 Y. Kohsaka, K. Nakazono, Y. Koyama, S. Asai and T. Takata, *Angew. Chem. Int. Ed*. 2011, **50**, 4872–4875.
24 W. Jiang, H. D. F. Winkler and C. A. Schalley, *J. Am. Chem. Soc*. 2008, **130**, 13852–13853.
25 M. Zhang, S. Li, S. Dong, J. Chen, B. Zheng and F. Huang, *Macromolecules*. 2011, **44**, 9629–9634.
26 Z. Zhang, C. Han, G. Yu and F. Huang, *Chem. Sci*. 2013, **3**, 3026–3031.
27 K. Kim, *Chem. Soc. Rev*. 2002, **31**, 96–107.
28 X. Xiao, L. He, Z. Tao, S. F. Xue, Q. J. Zhu and A. Day, *Supramol. Chem*. 2010, **22**, 194–201.
29 X. Xiao, J. X. Liu, Z. F. Fan, K. Chen, Q. J. Zhu, S. F. Xue and Z. Tao, *Chem. Commun.* 2010, **46**, 3741–3743.
30 X. Xiao, Q. Wang, Y. H. Yu, Z. Y. Xiao, Z. Tao, S. F. Xue, Q. J., J. X. Liu and X. H. Liu, *Eur. J. Org. Chem.* 2011, 2366–2371.
31 X. J. Cheng, L. L. Liang, K. Chen, N. N. Ji, X. Xiao, J. X. Zhang, Q. J. Zhu S. F. Xue, X. L. Ni and Z. Tao, *Angew. Chem., Int. Ed.* 2013, **52**, 7252–7255.
32 Cornelia Bohne, *Chem. Soc. Rev*. 2014, **43**, 4037–4050.
33 X. L. Ni, X. Xiao, H. Cong, Q. J. Zhu, S. F. Xue and Z. Tao, *Acc. Chem. Res*. 2014, **47**(4), 1386–1395.
34 Y. J. Zhao, S. F. Xue, Q. J. Zhu, Z. Tao, J. X. Zhang, Z. B. Wei, L. S. Long, M. L. Hu, H. P. Xiao and A. I. Day, *Chin. Sci. Bull.* 2004, **49**, 1111–1116.
35 J. P. Zeng, H. Cong, K. Chen, Z. Tao, S. F. Xue, Q. J. Zhu, Y. Q. Zhang and J. X. Liu, *Inorg. Chem.* 2011, **50**, 6521–6525.
36 X. Xiao, Q. H. Hu, Z. U. Tao, Y. Q. Zhang, S. F. Xue, Q. J. Zhu and G. Wei, *Chem. Phys. Lett*. 2011, **514**, 317–320.
37 X. Xiao, J. S. Sun and J. Z. Jiang , *Chem. Eur. J*. 2013, **19**, 16891–16896.
38 X. Xiao, S. C. Tu, S. F. Xue, Q. J. Zhu, Z. Tao, J. X. Zhang and G. Wei, *Chem. J. Chinese U.* 2013, **2**, 354–358.
39 X. Xiao, W. J. Li and J. Z. Jiang, *Inorg. Chem. Commun*. 2013, **35**, 156–159.
40 X. Xiao, S. C. Tu, S. F. Xue, Q. J. Zhu, Z. Tao, J. X. Zhang and G. Wei, *Chemical Journal of Chinese Universities*, 2013, **34**, 354–358.
41 R. L. Lin, W. Q. Sun, W. R. Yao, J. Zhu and J. X. Liu, *RSC Adv.*, 2014, **4**, 18323–18328.